 SID, vol.1, no.1, pp.1-20, 2005

Applications of DTALE: Damage Tolerance Analysis and Life Enhancement [3-D Non-plannar Fatigue Crack Growth]

S. N. Atluri [1]

Abstract: The solution of three-dimensional cracks (arbitrary surfaces of discontinuity) in solids and structures is considered. The BEM, developed based on the symmetric Galerkin BIEs, is used for obtaining the fracture solutions at the arbitrary crack-front. The finite element method is used to model the uncracked global (built-up) structure for obtaining the stresses in an otherwise uncracked body. The solution for the cracked structural component is obtained in an iteration procedure, which alternates between FEM solution for the uncracked body, and the SGBEM solution for the crack in the local finite-sized subdomain. In addition, some crack growth models are used to advance the crack front in fatigue and other stable-carck-growth situations. The crack-surface mesh is also changed correspondingly in the BEM model, while the FEM model for the uncracked structure is kept unchanged. The automatic crack growth analysis is achieved by repeating the fracture analysis, and the life of the structural components is estimated. Furthermore, the initial crack size and shape in a structure, as emanating from a microscopic defect, can be determined by utilizing the automatic crack-growth feature. Some state-of-the-art numerical solutions are also presented to indicate the type of problems that can now be solved using currently available techniques. All these methodologies are embedded in a user-friendly software, DTALE (Damage Tolerance Analysis and Life Enhancement), which is available for commercial use , in the safety evaluation and life-estimation of a variety of structures. Life enhancement methodologies with deliberate introduction of residual stress-fields, is also a feature of DTALE.

keyword: damage tolerance analysis, life enhancement, arbitrary 3D surface crack, finite element method, symmetric Galerkin boundary element method, the alternating method.

1 Introduction

The calculation of fracture mechanics parameters (such as the stress intensity factors of Modes I, II and III), for arbitrary non-planar three-dimensional surface and internal cracks, remains an important task in the structural integrity assessment and damage tolerance analysis [Atluri (1997)]. The three-dimensional stress analyses of crack configurations have received a lot of attention in the last two decades. Various methods have been investigated to obtain the stress-intensity factors for surface cracks: the finite element method (FEM), the boundary element method (BEM), the coupled FEM-BEM method and the FEM-BEM alternating method, as summarized in [Atluri (1986)]. They were used successfully for this purpose.

The finite element method is generally regarded as the most powerful numerical method since it can handle complicated geometries and loading conditions. The fracture mechanics problems are solved by using singularity elements [Tan, Newman and Bigelow (1996); Raju and Newman (1979)] or displacement hybrid elements [Atluri and Kathireasan (1975)], or by using certain path-independent and domain-independent integrals based on conservative laws of continuum mechanics [Nikishkov and Atluri (1987); Shivakumar and Raju (1992)]. Unfortunately, these methods require an explicit finite-element modeling of cracks, such as in HKS/ABAQUS. They encounter a serious difficulty in the mesh generation when they are applied to three-dimensional problems, with the extremely high human labor cost for creating appropriate meshes for cracks in structural components of arbitrary geometry. In addition, it is almost impossible to keep creating the meshes with high quality, during crack propagation.

It is well known that boundary element methods (BEM) have distinct advantages over domain approaches in solving of linear elastic fracture mechanics problems. In

[1] Center for Aerospace Research & Education, University of California, Irvine, 5251 California Avenue, Suite 140 Irvine, CA, 92612, USA

BEM, the mesh should be generated only for the boundary of the structure, and for the crack surface. Consequently, it is simpler to create a boundary element mesh, in comparison to a finite element mesh for a body with a crack. The traditional (collocation) boundary element method has certain features, which make it suitable for the solution of crack problems. Recent publications on the dual boundary element method [Cisilino and Aliabadi (1999)] can serve as an example of application of traditional BEM to linear and non-linear fracture mechanics problems. The symmetric Galerkin boundary element method (SGBEM) [Han and Atluri (2002, 2003a)] has been recently developed, based on a weakly singular weak-form of integral equations. The system matrix shows symmetry and sign-definiteness. The SGBEM overcomes some drawbacks of the traditional boundary element methods, including the nonsymmetrical matrix of the equation system, and the hypersingular kernels. Another advantage of the SGBEM is that, after a special transformation to remove the singularity from kernels, the system matrices can be integrated with the use of usual Gaussian quadrature rule [Andra (1998); Erichsen and Sauter (1998)]. But from the numerical point of view, the SGBEM, like all BEM approaches, entails fully populated coefficient matrices, which hinders their application to large-scale problems with complex geometry.

The coupled FEM-BEM approaches are also proposed for fracture analyses by limiting the employment of the BEM to the fractured region [Keat, Annigeri and Cleary (1988); Frangi and Novati (2002)]. The SGBEM shows its special advantage in such a coupled approach, with its symmetric system matrices and sign-definiteness. An obvious disadvantage of this approach is that, both the mesh of fractured region for BEM and the mesh for the remaining part for FEM should be modified when it is necessary to analyze cracks of different sizes and locations, including crack-growth.

The alternating method, generally known as the Schwartz-Neumann alternating method, obtains the solution on a domain that is the intersection of two other overlapping domains [Kantorovich and Kriylov (1964)]. The procedure has been applied to fracture mechanical analyses. Normally the two domains are defined to be: one, a finite body without the crack; and the second, an infinite body with cracks. The solution is obtained by iterating between the solution for the uncracked finite body (usually using FEM), and the cracks in an inifinite region obtained with collocation BEM or SGBEM. Each solution can be solved by various methods [Atluri (1997); Nishioka and Atluri (1983); Vijaykumar and Atluri (1981); Wang and Atluri (1996)]. For a complex geometry with the arbitrary cracks, the alternating procedure has been implemented by iterating between the FEM and the SGBEM [Nikishkov, Park and Atluri (2001); Han and Atluri (2002)]. In [Nikishkov, Park and Atluri (2001)], two solutions are employed iteratively: 1. The FEM solution for stresses in the uncracked global structure; 2. The SGBEM solution for the crack in an inifinite body – thus only the crack surfaces are modeled in the SGBEM. This approach has been applied to the embedded cracks with high accuracy. It also demonstrated the flexibility in choosing the overlapping domains for different crack configurations. From a computational point of view, it also shows its efficiency in saving both computational and human labor time, by leveraging the existing FE models. This work has been extended in [Han and Atluri (2002)], in which he solution is obtained by alternating between two finite domains: the global uncracked structure is solved by using the FEM, and a local cracked subdomain is solved by using the SGBEM. It eliminates the need for evaluating the singular integral of tractions at the free surface, during the alternating procedure when surface crack problems are considered. At the same time, it limits the employment of the SGBEM only for the local cracked subdomain, and reduces the computational cost and memory requirements, since the SGBEM entails the fully populated system matrix. In additon, the alternating method may be also extended for the crack problems by using the truely meshless methods, through the meshless local Petrov-Galerkin approach (MLPG), pioneered by Atluri and his colleagues [Atluri(2004); Atluri, Han and Shen(2003); Han and Atluri (2003b, 2004a, 2004b)].

The present work discusses the recent development of the alternating method based on FEM and SGBEM, embedded in a commercial-quality software, DTALE: "Damage Tolerance Analysis and Life Enhancement ". With DTALE, the BEM is applied only for the local crack subdomain, and reduces the computational cost and memory requirements. With the use of the built-in FEM solver, DTALE can handle much more complex structural components than pure BEM solvers. In addition, DTALE provides an interface to commercial FEM codes (such as NASTRAN, ABAQUS and MARC) to retrieve the FEM solutions of uncracked structures. From the modeling point of view, this approach makes the full use of the existing FE models to avoid any model regeneration, which is extremely high in human labor cost. The presently proposed procedure is demonstrated by solving both the embedded and surface cracks problems. The stress intensity factors are calculated and compared with the earlier published solutions. The good agreements show that the FEM-SGBEM alternating method between two finite domains is very efficient and highly accurate for 3D arbitrary crack problems. DTALE is also used to solve the problem of mixed-mode fatigue-growth of an initially-semi-circular surface flaw which is inclined to the direction of tensile loading in a thick plate. In addition, the automatic determination of the initial crack is also demonstrated by using the DTALE.

2 Formulation of the non-hyper-singular symmetric Galerkin boundary element method

The non-hypersingular displacement and traction BIEs for a linear elastic, homogeneous, isotropic solid, are summarized in this section. Consider a linear elastic, homogeneous, isotropic body in a domain Ω, with a boundary $\partial\Omega$. The Lame' constants of the linear elastic isotropic body are λ and μ; and the corresponding Young's modulus and Poisson's ratio are E and υ, respectively. We use Cartesian coordinates ξ_i, and the attendant base vectors $\mathbf{e}_i$, to describe the geometry in Ω. The solid is assumed to undergo infinitesimal deformations. The equations of balance of linear and angular momentum can be written as:

$$\nabla\cdot\boldsymbol{\sigma}+\mathbf{f}=\mathbf{0};\quad \boldsymbol{\sigma}=\boldsymbol{\sigma}^t;\quad \nabla=\mathbf{e}_i\frac{\partial}{\partial\xi_i} \tag{1}$$

The constitutive relations of an isotropic linear elastic homogeneous solid are:

$$\boldsymbol{\sigma}=\lambda\boldsymbol{I}(\nabla\cdot\boldsymbol{u})+2\mu\,\boldsymbol{\varepsilon} \tag{2}$$

It is well known that the displacement vector, which is a continuous function of $\boldsymbol{\xi}$, can be derived, in general, from the Galerkin-vector-potential $\boldsymbol{\varphi}$ such that:

$$\boldsymbol{u}=\nabla^2\boldsymbol{\varphi}-\frac{1}{2(1-\upsilon)}\nabla(\nabla\cdot\boldsymbol{\varphi}) \tag{3}$$

Consider a point unit load applied in an arbitrary direction $\mathbf{e}^p$ at a generic location $\mathbf{x}$ in a linear elastic isotropic homogeneous infinite medium. It is well-known that the displacement solution is given by the Galerkin-vector-displacement-potential:

$$\boldsymbol{\varphi}^{*p}=(1-\upsilon)F^*\mathbf{e}^p \tag{4}$$

in which F^* is a scalar function, as

$$F^*=\frac{r}{8\pi\mu(1-\upsilon)}\quad \text{for 3D problems} \tag{5}$$

and

$$F^*=\frac{-r^2\ln r}{8\pi\mu(1-\upsilon)}\quad \text{for 2D problems} \tag{6}$$

where $r=\|\boldsymbol{\xi}-\mathbf{x}\|$

The corresponding displacements are derived, by using Eq. (3), as:

$$u_i^{*p}(\mathbf{x},\boldsymbol{\xi})=(1-\upsilon)\delta_{pi}F^*_{,kk}-\frac{1}{2}F^*_{,pi} \tag{7}$$

and the gradients of the displacements in (7) are:

$$u_{i,j}^{*p}(\mathbf{x},\boldsymbol{\xi})=(1-\upsilon)\delta_{pi}F^*_{,kkj}-\frac{1}{2}F^*_{,pij} \tag{8}$$

By taking the fundamental solution $u_i^{*p}(\mathbf{x},\boldsymbol{\xi})$ in Eq. (7) as the test functions, one may write the weak-form of the equilibrium Eq. (1). The traditional displacement BIE can be written as,

$$\begin{aligned} u_p(\mathbf{x})=&\int_{\partial\Omega}t_j(\boldsymbol{\xi})u_j^{*p}(\mathbf{x},\boldsymbol{\xi})\,dS\\ &-\int_{\partial\Omega}n_i(\boldsymbol{\xi})u_j(\boldsymbol{\xi})\sigma_{ij}^{*p}(\mathbf{x},\boldsymbol{\xi})\,dS \end{aligned} \tag{9}$$

Where σ_{ij}^{*p} is the stress field of the fundamental solution, as

$$\begin{aligned} \sigma_{ij}^{*p}(\mathbf{x},\boldsymbol{\xi})&\equiv E_{ijkl}u_{k,l}^{*p}\\ &=\mu[(1-\upsilon)\delta_{pi}F^*_{,kkj}+\upsilon\delta_{ij}F^*_{,pkk}-F^*_{,pij}]\\ &\quad+\mu(1-\upsilon)\delta_{pj}F^*_{,kki} \end{aligned} \tag{10}$$

Instead of the ***scalar*** weak form of Eq. (1), as used for the displacement BIE, we may also write a ***vector*** weak form of Eq. (1), by using the tensor test functions $u_{i,j}^{*p}(\mathbf{x},\boldsymbol{\xi})$ in Eq. (8) [as originally proposed in Okada, Rajiyah, and Atluri (1989), Okada and Atluri(1994)], and derive a non-hypersingular integral equation for tractions in a linear elastic solid [Han and Atluri (2003)],

$$
\begin{aligned}
-t_b(\mathbf{x}) = &\int_{\partial\Omega} t_q(\boldsymbol{\xi}) n_a(\mathbf{x}) \sigma_{ab}^{*q}(\mathbf{x},\boldsymbol{\xi})\, dS \\
&+ \int_{\partial\Omega} D_p u_q(\boldsymbol{\xi}) n_a(\boldsymbol{x}) \Sigma_{abpq}^{*}(\mathbf{x},\boldsymbol{\xi})\, dS
\end{aligned} \tag{11}
$$

where Σ^*_{abpq} is another derived kernel function, which were first given by Han and Atluri [2]

$$
\begin{aligned}
\Sigma^*_{ijpq}(\mathbf{x},\boldsymbol{\xi}) &= E_{ijkl} e_{nlp} \sigma^{*k}_{nq}(\mathbf{x},\boldsymbol{\xi}) \\
&= \mu^2[(e_{inp}F_{,jqn} - e_{inp}\delta_{jq}F_{,bbn} \\
&\quad + e_{int}e_{tqk}e_{jpm}F_{,kmn}) \\
&\quad + \upsilon(e_{inq}\delta_{jp}F_{,bbn} + e_{jnq}\delta_{ip}F_{,bbn})]
\end{aligned} \tag{12}
$$

and the surface tangential operator D_t is defined as,

$$
D_t = n_r e_{rst}\frac{\partial}{\partial \xi_s} \tag{13}
$$

The singularity of $u_i^{*p}$is $O(1/r)$, as the second derivatives of $F^*$are included. The singularities are $O(1/r^2)$ for σ^{*p}_{ij} and Σ^*_{abpq} because of the third derivatives of F^*. Thereafter, the displacement and traction BIEs in Eqs. (9) and (11) have the non-hyper-singularities only. It should be noted that these two integral equations for $u_p(\mathbf{x})$ and $t_b(\mathbf{x})$ are derived independently of each other. On the other hand, if we derive the integral equation for the displacement-gradients, by directly differentiating $u_p(\mathbf{x})$ in Eq. (9), a hyper-singularity is clearly introduced due to the forth derivatives.

Furthermore, Eqs. (9) and (11) may be satisfied in weak-*forms* over the boundary surface $\partial\Omega$, by using a Galerkin scheme. One may obtain the symmetric Galerkin displacement and traction BIEs after applying Stokes' theorem, as

$$
\begin{aligned}
&\frac{1}{2}\int_{\partial\Omega} \hat{t}_p(\mathbf{x}) u_p(\mathbf{x}) dS_x \\
&\quad = \int_{\partial\Omega} \hat{t}_p(\mathbf{x}) dS_x \int_{\partial\Omega} t_j(\boldsymbol{\xi}) u_j^{*p}(\mathbf{x},\boldsymbol{\xi})\, dS_\xi \\
&\quad + \int_{\partial\Omega} \hat{t}_p(\mathbf{x}) dS_x \int_{\partial\Omega} D_i(\boldsymbol{\xi}) u_j(\boldsymbol{\xi}) G_{ij}^{*p}(\mathbf{x},\boldsymbol{\xi})\, dS_\xi \\
&\quad + \int_{\partial\Omega} \hat{t}_p(\mathbf{x}) dS_x \int_{\partial\Omega}^{CPV} n_i(\boldsymbol{\xi}) u_j(\boldsymbol{\xi}) \phi_{ij}^{*p}(\mathbf{x},\boldsymbol{\xi})\, dS_\xi
\end{aligned} \tag{14}
$$

$$
\begin{aligned}
&-\frac{1}{2}\int_{\partial\Omega} t_b(\mathbf{x}) \hat{u}_b(\mathbf{x}) dS_x \\
&\quad = \int_{\partial\Omega} D_a \hat{u}_b(\mathbf{x}) dS_x \int_{\partial\Omega} t_q(\boldsymbol{\xi}) G_{ab}^{*q}(\mathbf{x},\boldsymbol{\xi})\, dS_\xi \\
&\quad - \int_{\partial\Omega} t_q(\boldsymbol{\xi})\, dS_\xi \int_{\partial\Omega}^{CPV} n_a(\mathbf{x}) \hat{u}_b(\mathbf{x}) \phi_{ab}^{*q}(\mathbf{x},\boldsymbol{\xi}) dS_x \\
&\quad + \int_{\partial\Omega} D_a \hat{u}_b(\mathbf{x}) dS_x \int_{\partial\Omega} D_p u_q(\boldsymbol{\xi}) H_{abpq}^{*}(\mathbf{x},\boldsymbol{\xi})\, dS_\xi
\end{aligned} \tag{15}
$$

where G^{*p}_{ij}, ϕ^{*p}_{ij} and H^*_{ijpq} are kernel functions and given as [Han and Atluri (2003)],

For 3D problems,

$$
G_{ij}^{*p}(\mathbf{x},\boldsymbol{\xi}) = \frac{1}{8\pi(1-\upsilon)r}[(1-2\upsilon)e_{ipj} + e_{ikj}r_{,k}r_{,p}] \tag{16a}
$$

$$
\phi_{ij}^{*p}(\mathbf{x},\boldsymbol{\xi}) = \frac{1}{4\pi r^2}\delta_{pj}r_{,i} \tag{16b}
$$

$$
\begin{aligned}
H^*_{ijpq}(\mathbf{x},\boldsymbol{\xi}) = \frac{\mu}{8\pi(1-\upsilon)r}&[4\upsilon\delta_{iq}\delta_{jp} - \delta_{ip}\delta_{jq} \\
&- 2\upsilon\delta_{ij}\delta_{pq} + \delta_{ij}r_{,p}r_{,q} + \delta_{pq}r_{,i}r_{,j} \\
&- 2\delta_{ip}r_{,j}r_{,q} - \delta_{jq}r_{,i}r_{,p}]
\end{aligned} \tag{16c}
$$

For 2D problems,

$$
G_{ij}^{*p}(\mathbf{x},\boldsymbol{\xi}) = \frac{1}{4\pi(1-\upsilon)}[-(1-2\upsilon)\ln r\, e_{ipj} + e_{ikj}r_{,k}r_{,p}] \tag{17a}
$$

$$
\phi_{ij}^{*p}(\mathbf{x},\boldsymbol{\xi}) = \frac{1}{2\pi r}\delta_{pj}r_{,i} \tag{17b}
$$

$$
\begin{aligned}
H^*_{ijpq}(\mathbf{x},\boldsymbol{\xi}) = \frac{\mu}{4\pi(1-\upsilon)}&[-4\upsilon\ln r\delta_{iq}\delta_{jp} \\
&+ \ln r\delta_{ip}\delta_{jq} + 2\upsilon\ln r\delta_{ij}\delta_{pq} \\
&+ \delta_{ij}r_{,p}r_{,q} + \delta_{pq}r_{,i}r_{,j} \\
&- 2\delta_{ip}r_{,j}r_{,q} - \delta_{jq}r_{,i}r_{,p}]
\end{aligned} \tag{17c}
$$

For a crack problem shown in Fig. 1, the boundary surface $\partial\Omega$ includes the prescribed displacement surface S_u, the prescribed traction surface S_t, and the crack surface S_c. We apply the weak-form displacement integral equation on the prescribed displacement boundary surfaces S_u and obtain the formulation as:

$$
\begin{aligned}
&\frac{1}{2}\int_{S_u} \hat{t}_p(\mathbf{x}) u_p(\mathbf{x}) dS_x \\
&\quad = \int_{S_u} \hat{t}_p(\mathbf{x}) dS_x \int_{\partial\Omega} t_j(\boldsymbol{\xi}) u_j^{*p}(\mathbf{x},\boldsymbol{\xi})\, dS_\xi \\
&\quad + \int_{S_u} \hat{t}_p(\mathbf{x}) dS_x \int_{\partial\Omega} D_i(\boldsymbol{\xi}) u_j(\boldsymbol{\xi}) G_{ij}^{*p}(\mathbf{x},\boldsymbol{\xi})\, dS_\xi \\
&\quad + \int_{S_u} \hat{t}_p(\mathbf{x}) dS_x \int_{\partial\Omega}^{CPV} n_i(\boldsymbol{\xi}) u_j(\boldsymbol{\xi}) \phi_{ij}^{*p}(\mathbf{x},\boldsymbol{\xi})\, dS_\xi
\end{aligned} \tag{18}
$$

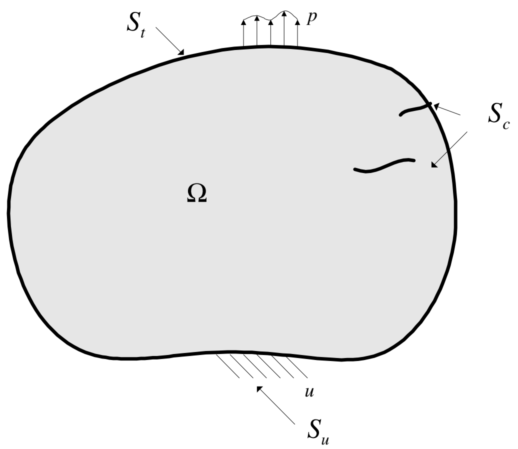

Figure 1 : A linear elastic isotropic domain containing cracks (Original problem)

We apply the weak-form traction integral equation on the prescribed traction boundary surfaces S_t and obtain the similar formulation as:

$$\begin{aligned}
&-\frac{1}{2}\int_{S_t} t_b(\mathbf{x})\hat{u}_b(\mathbf{x})dS_x \\
&=\int_{S_t} D_a\hat{u}_b(\mathbf{x})dS_x\int_{S_t+S_u} t_q(\boldsymbol{\xi})G^{*q}_{ab}(\mathbf{x},\boldsymbol{\xi})\, dS_\xi \\
&-\int_{S_t+S_u} t_q(\boldsymbol{\xi})\, dS_\xi \int^{CPV}_{S_t} n_a(\mathbf{x})\hat{u}_b(\mathbf{x})\phi^{*q}_{ab}(\mathbf{x},\boldsymbol{\xi})dS_x \\
&+\int_{S_t} D_a\hat{u}_b(\mathbf{x})dS_x\int_{\partial\Omega} D_p u_q(\boldsymbol{\xi})H^*_{abpq}(\mathbf{x},\boldsymbol{\xi})\, dS_\xi
\end{aligned} \tag{19}$$

We also apply the weak-form traction integral equation on the crackS_c, which are conceived as a set of prescribed traction boundary surfaces. We have

$$\begin{aligned}
&-\frac{1}{2}\int_{S_c} t_b(\mathbf{x})\hat{u}_b(\mathbf{x})dS_x \\
&=\int_{S_c} D_a\hat{u}_b(\mathbf{x})dS_x\int_{S_t+S_u} t_q(\boldsymbol{\xi})G^{*q}_{ab}(\mathbf{x},\boldsymbol{\xi})\, dS_\xi \\
&-\int_{S_t+S_u} t_q(\boldsymbol{\xi})\, dS_\xi \int^{CPV}_{S_c} n_a(\mathbf{x})\hat{u}_b(\mathbf{x})\phi^{*q}_{ab}(\mathbf{x},\boldsymbol{\xi})dS_x \\
&+\int_{S_c} D_a\hat{u}_b(\mathbf{x})dS_x\int_{\partial\Omega} D_p u_q(\boldsymbol{\xi})H^*_{abpq}(\mathbf{x},\boldsymbol{\xi})\, dS_\xi
\end{aligned} \tag{20}$$

The SGBEM requires the C_0 continuous trial and testing functions over the boundary surface $\partial\Omega = S_u \cup S_t \cup S_c$. This can be satisfied after discretization. Special attention should be paid to the crack surfaces. The displacement discontinuities, $u(x) = u^+(x^+) - u^-(x^-)$, must be zero around the crack fronts where $u^+(x^+) = u^-(x^-)$. A special treatment is also required to enforce the C_0 continuities for the surface cracks that intersect the normal boundary surface $S_u \cup S_t$. In the present work, quarter-point singular elements are adopted and the displacement discontinuities are set to zero explicitly for the crack front. In addition, the weak-form can be also written for the local sub boundary, by using the generate MLPG approach. It has been presented in [Alturi, Han and Shen (2003)].

3 Schwartz-Neumann Alternating Method

The Schwartz-Neumann alternating method is based on the superposition principle. The solution on a given domain is the sum of the solutions on two other overlapping domains. The alternating method converges unconditionally when there are only traction boundary conditions specified on the body. In the present work, the overlapping domains are the given finite domain, but without the cracks; a local portion of the original given domain as described below. The local subdomain can be selected to include only the traction boundary conditions so that the alternating procedure converges unconditionally. To take advantages of both the FEM and SGEM, the FEM, which is a robust method for large-scale elastic problems, is used to solve the whole uncracked global structure. The SGBEM, which is most suitable the crack analyses, is used for modeling a local finite-sized subdomain containing embedded or surface cracks. The size of SGBEM domain is also limited in order to improve the computational efficiency, by avoiding an overly-large fully populated system matrix.

We consider a structure containing cracks, as shown in Fig. 1. The crack surfaces are denoted collectively as S_c. The alternating method uses the following two problems to solver the original one. Let us define that the domain for the FEM, denoted as Ω^{FEM} in Fig. 2(a), is the same as the original domain Ω but no cracks are included. All the prescribed tractions p are applied to the FEM domain on S_t^{FEM}, as well as all the prescribed displacement u on S_u^{FEM}. Another domain Ω^{SGBEM} is defined for the SGBEM as shown in Fig. 2(b), which is a local finite-sized subdomain containing all the cracks. It is clear that the same crack surfaces are inherited from the original ones, as S_c^{SGBEM}. We define the boundary conditions in a way that the shared overall boundary between these two domains is defined as the traction free surface of the SGBEM domain, denoted as S_t^{SGBEM} with

$p^{SGBEM} = 0$. The intersection surface S^I is treated as the boundary of the SGBEM domain with the prescribed displacements, denoted as S_u^{SGBEM}. We can also restrict all prescribed displacements, u^{SGBEM}, to be zero on S_u^{SGBEM}. One obvious advantage of this approach is that two overlapping domains are limited to the local portion containing the cracks, without any restriction to the remaining portion. This distinguishing feature makes it possible that all other structure elements can be used in the FEM domain, which are widely used in industry. It also allows the present alternating approach to be implemented within any commercial FEM solver without any restriction. Another advantage is that the independence of the crack model and finite element model of the body allows one to easily change the crack model in order to simulate crack growth or perform the parametric study.

To solve the original problem, the superposition of the two alternate problems, FEM and SGBEM, yields the original solution for the prescribed displacements u and tractions p with cracks. The detailed procedures are described as follows.

1. Using FEM, solve the problem on domain Ω^{FEM} with all externally prescribed displacements and tractions, but without the cracks. The tractions on crack surfaces S_c^{SGBEM} can be obtained as $p_c^{SGBEM} \equiv -p_c^{FEM}$.

2. Using SGBEM, solve the local problem on domain Ω^{SGBEM} only with the tractions on the crack surface. The prescribed displacements u^{SGBEM}on S_u^{SGBEM} are set to zero as well as the zero prescribed tractions p^{SGBEM}on S_t^{SGBEM}. The only loads are the non-zero tractions on the crack surfaces, i.e., p_c^{SGBEM}on S_c^{SGBEM}. Then the tractions on the intersection surface S^I are obtained as a part of the SGBEM solution explicitly, denoted as p_u^{SGBEM}on S_u^{SGBEM}.

3. Applying the tractions on the intersection surface as the residual forces to the FEM domain, denoted as $p^{FEM} \equiv -p_u^{SGBEM}$on S^I in Fig. 2(c), re-solve the FEM problem and obtain the traction p_c^{SGBEM} on crack surfaces S_c^{SGBEM}.

4. Repeat steps 2 and 3 until the residual load $p^{FEM}$is small enough.

5. By adding the SGBEM solution to the FEM one, the original one is obtained.

We now examine the solution with the given boundary and loading conditions for the original problem (denoted by superscript Org):

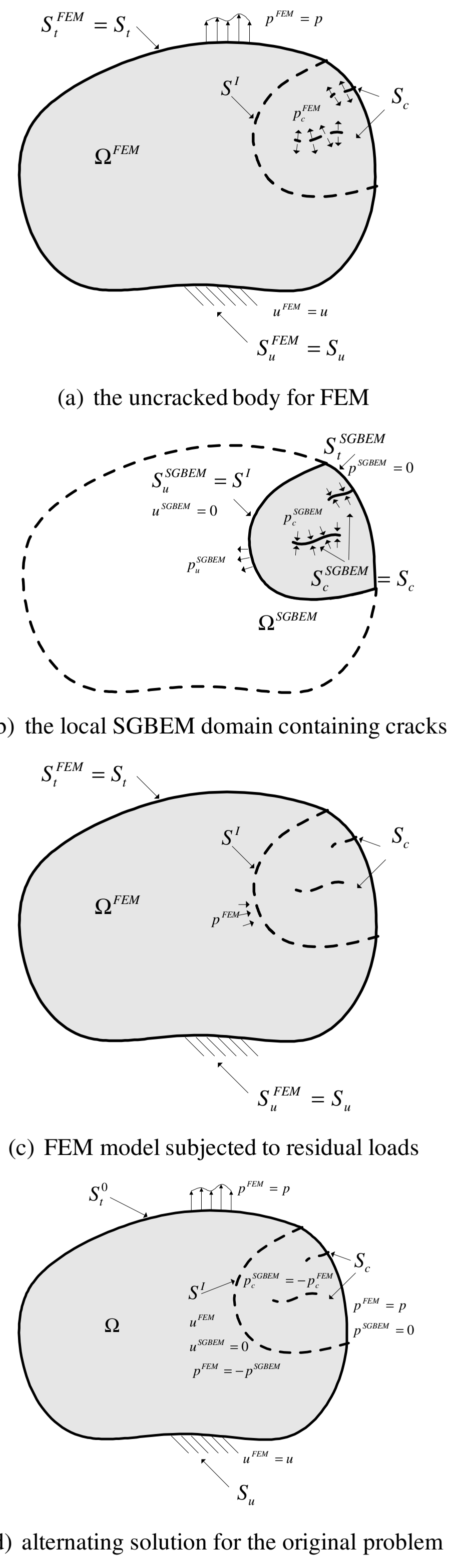

(a) the uncracked body for FEM

(b) the local SGBEM domain containing cracks

(c) FEM model subjected to residual loads

(d) alternating solution for the original problem

Figure 2 : Superposition principle for FEM-SGBEM alternating method

i) for the given traction on S_t, we have $p^{FEM} = p$ and $p^{SGBEM} = 0$ and get

$$p^{Org} = p^{FEM} + p^{SGBEM} = p \qquad \text{on} \quad S_t \tag{21}$$

ii) for the given displacement on S_u, the SGBEM domain does not contain any portion of S_u and thus, we obtain

$$u^{Org} = u^{FEM} = u \qquad \text{on} \quad S_t \tag{22}$$

iii) for the crack surface S_c, we define that tractions for SGBEM modelp_c^{SGBEM} equal to $-p_c^{FEM}$ from the FEM solution, and thus the tractions on crack surfaces are zero as in the original problem, i.e.,

$$p_c^{Org} = p_c^{FEM} + p_c^{SGBEM} = 0 \qquad \text{on} \quad S_c \tag{23}$$

iv) for the intersection surface S^I, we define that the residual tractions on FEM model p^{FEM} equals to $-p^{SGBEM}$ from the SGBEM solution, and obtain

$$p_c^{Org} = p_c^{FEM} + p_c^{SGBEM} = 0 \qquad \text{on} \quad S^I \tag{24}$$

We also specify that the zero displacements for the SGBEM model, i.e. $u^{SGBEM} = 0$ on S^I, and thus, there no displacement discontinuities along the intersection surface,

$$u^{Org} = u^{FEM} \qquad \text{on} \quad S^I \tag{25}$$

As shown in Fig. 2 (d), the solution obtained here satisfies all the boundary and loading conditions for the original problem. From the uniqueness of the elastic linear problem, we obtain the solution for the original problem

From a computational point of view, the present approach is very efficient in saving the CPU time. This results from two reasons. The first reason is that some terms for SGBEM equations are ignored, and Eqs. (18), (19) and 3 can be simplified as follows

For weak-form displacement integral on S_u^{SGBEM}

$$\begin{aligned}0 &= \int_{S_u} \hat{t}_p(\mathbf{x})dS_x \int_{S_u} t_j(\boldsymbol{\xi})u_j^{*p}(\mathbf{x},\boldsymbol{\xi})\, dS_\xi \\ &+ \int_{S_u} \hat{t}_p(\mathbf{x})dS_x \int_{S_t+S_c} D_i(\boldsymbol{\xi})u_j(\boldsymbol{\xi})G_{ij}^{*p}(\mathbf{x},\boldsymbol{\xi})\, dS_\xi \\ &+ \int_{S_u} \hat{t}_p(\mathbf{x})dS_x \int_{S_t+S_c}^{CPV} n_i(\boldsymbol{\xi})u_j(\boldsymbol{\xi})\phi_{ij}^{*p}(\mathbf{x},\boldsymbol{\xi})\, dS_\xi\end{aligned} \tag{26}$$

For weak-form traction integral on S_t^{SGBEM}

$$\begin{aligned}0 &= \int_{S_t} D_a\hat{u}_b(\mathbf{x})dS_x \int_{S_u} t_q(\boldsymbol{\xi})G_{ab}^{*q}(\mathbf{x},\boldsymbol{\xi})\, dS_\xi \\ &- \int_{S_u} t_q(\boldsymbol{\xi})\, dS_\xi \int_{S_t}^{CPV} n_a(\mathbf{x})\hat{u}_b(\mathbf{x})\phi_{ab}^{*q}(\mathbf{x},\boldsymbol{\xi})dS_x \\ &+ \int_{S_t} D_a\hat{u}_b(\mathbf{x})dS_x \int_{S_t+S_c} D_p u_q(\boldsymbol{\xi})H_{abpq}^{*}(\mathbf{x},\boldsymbol{\xi})\, dS_\xi\end{aligned} \tag{27}$$

For weak-form traction integral on S_c^{SGBEM}

$$\begin{aligned}&-\frac{1}{2}\int_{S_c} t_b(\mathbf{x})\hat{u}_b(\mathbf{x})dS_x \\ &= \int_{S_c} D_a\hat{u}_b(\mathbf{x})dS_x \int_{S_u} t_q(\boldsymbol{\xi})G_{ab}^{*q}(\mathbf{x},\boldsymbol{\xi})\, dS_\xi \\ &- \int_{S_u} t_q(\boldsymbol{\xi})\, dS_\xi \int_{S_c}^{CPV} n_a(\mathbf{x})\hat{u}_b(\mathbf{x})\phi_{ab}^{*q}(\mathbf{x},\boldsymbol{\xi})dS_x \\ &+ \int_{S_c} D_a\hat{u}_b(\mathbf{x})dS_x \int_{S_t+S_c} D_p u_q(\boldsymbol{\xi})H_{abpq}^{*}(\mathbf{x},\boldsymbol{\xi})\, dS_\xi\end{aligned} \tag{28}$$

$$K_{eq} = \sqrt[4]{K_I^4 + 6K_I^2K_{II}^2 + K_{II}^4 + \frac{K_{III}^4}{(1-\upsilon)^2}} \tag{29}$$

The second reason is that the residual forces applied to the FEM problem are obtained as a part the SGBEM solution explicitly. There is no extra computer time to determine the forces, which is normally needed when the alternating procedure is performed between the solutions for the uncracked finite body and the infinite body containing cracks. The singular residual forces may be encountered when the surface cracks are included the later cases, which introduces the numerical errors during the alternating procedures. Therefore the surface crack solutions near the free surface are not accurate, which is well known as the boundary-layer effect. In some researches, the fictitious extended cracks are used with imaginary tractions to reduce such errors [Nishioka and Atluri (1983)]. Unfortunately, the fictitious extended portion and the imaginary tractions are hard to be defined when the arbitrary non-planar surface cracks are considered. In the present work, the original solution is obtained accurately by using the non-singular alternating method with the weak singular SGBEM.

4 Automatic crack growth

The crack growth analysis plays an important role in the damage tolerance analysis for determining the life of the

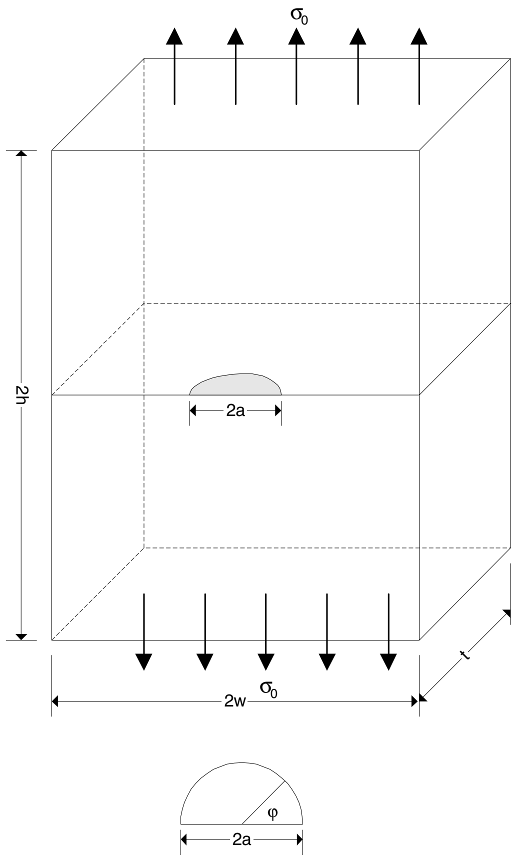

Figure 3 : a semi-circular crack in a plate under tension

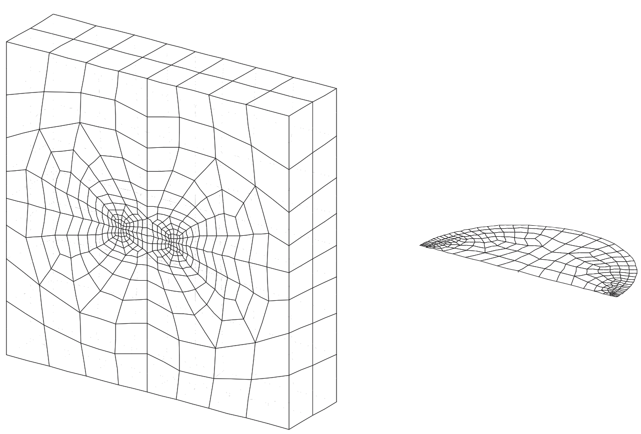

Figure 4 : Mesh of a semi-circular crack in a plate for the SGBEM

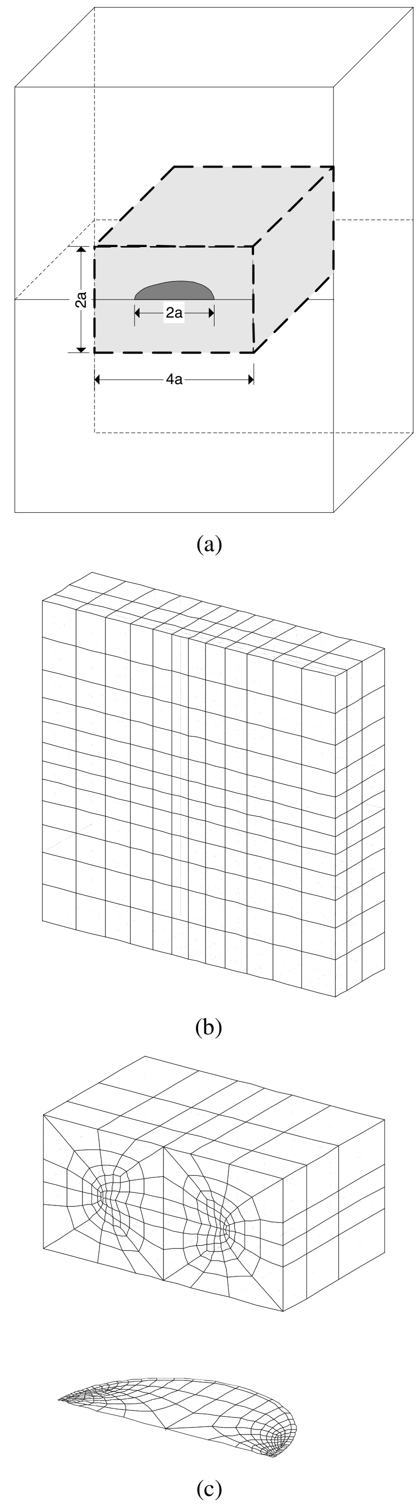

Figure 5 : Models of a semi-circular crack in a plate for FEM-SGBEM alternating method: (a) local finite body defined in the plate, (b) the FEM model without the crack and (c) the local SGBEM model with the crack

structure. Several models can be used to predict the direction and extension of cracks. The models for crack extension use in the equivalent K factorsfor the mixed mode and the stress ratio, such as the Paris, Walker and Forman fatigue models. In the current implementation,

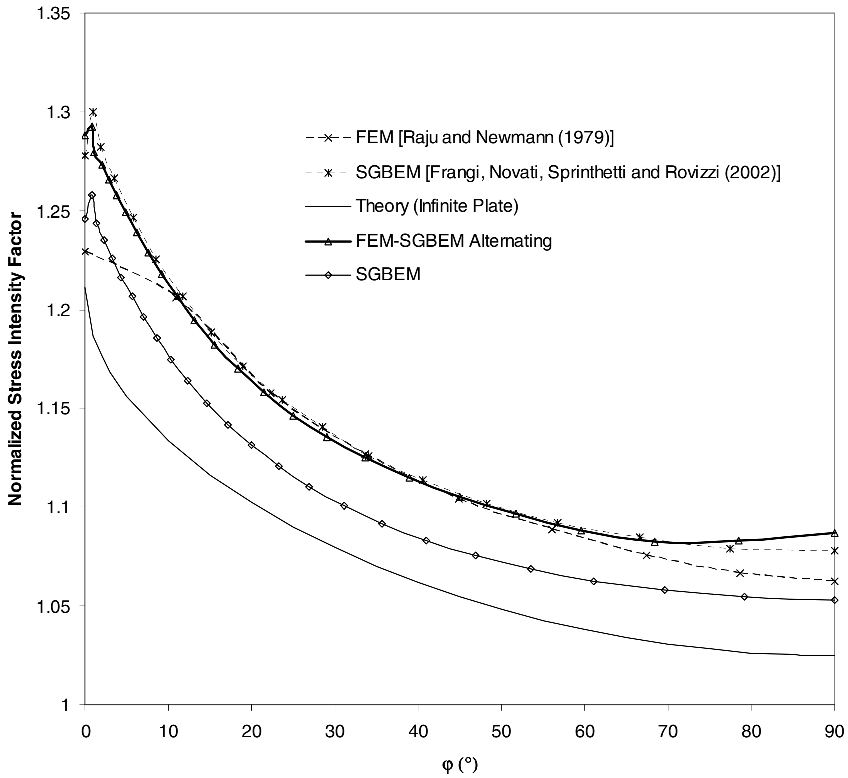

Figure 6 : Normalized stress intensity factors ($K_I/\sqrt{\pi a}$) for a semi-circular crack in a plate

the equivalent K factor is calculated as

Thereafter, the rate of crack extension is governed by the corresponding models as

$$\frac{da}{dN} = f(K_{eq}, R, \ldots) \tag{30}$$

The maximum circumfeential stress theory is used for the direction, as

$$K_I \sin\alpha + K_{II}(3\cos\alpha - 1) = 0 \tag{31}$$

Once the crack extension and direction are obtained, the crack can be advanced by adding another layer of the elements around the crack front to grow the crack. As one of the most important feature of the alternating method, the FEM model keeps unchanged and is solved only once during the crack growth because the models for the FEM and BEM are fully decoupled. It makes that the alternating method is very efficient for crack-growth problems. In addition, the mesh generation is robust because only the 3D surface mesh is required for the advanced crack surface, instead of embedding the new crack surface into a finite body.

5 Numerical Examples

5.1 *Semi-circular surface cracks*

In order to verify the accuracy of the present alternating method for treating surface cracks in finite bodies, we first consider a semi-circular surface crack in a plate as shown in Fig. 3. Uniform tensile stresses σ_0 are applied at two opposite faces of the plate in the direction perpendicular to the cracks. a is the radius of the semi circular crack. The plate configuration considered is characterized by the geometric ratios $\frac{h}{a} = 5$, $\frac{w}{a} = 5$ and $\frac{t}{a} = 2.5$. The passion ratio $\nu = 0.3$ is chosen.

We first use the SGBEM method to simulate the entire problem with the mesh shown in Fig. 4. Then we solve the problem with the alternating method. The FEM model is created for the uncracked body, shown in Fig. 5(b), with the uniform tensile stresses being applied at the top and bottom surfaces. The local SGBEM model is also created in the plate, shown in Fig. 5(a). It is similar to the model in Fig. 4 for pure SGBEM solution, so that we create the mesh for this local finite body with similar meshes for the boundary and crack surfaces. The front and back surfaces are free and others are the prescribed

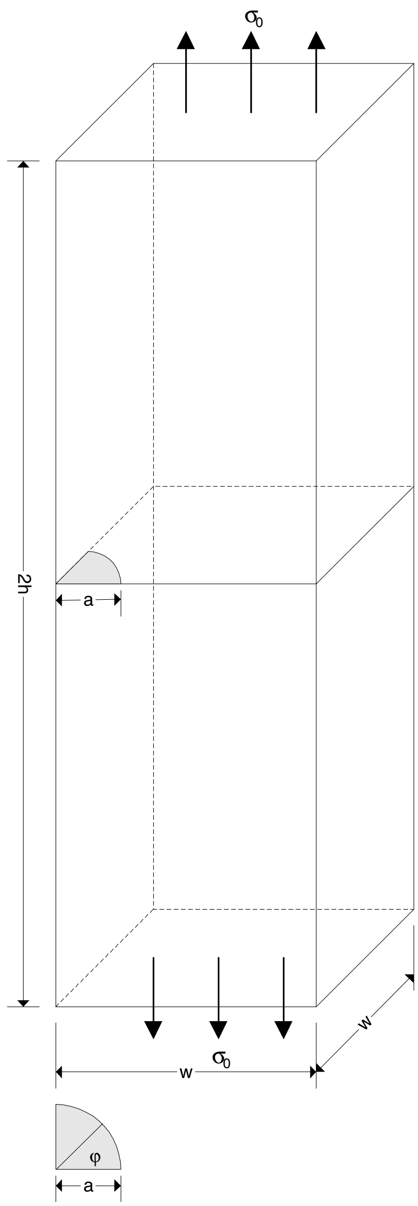

Figure 7 : a quarter-circular crack in a square bar under tension

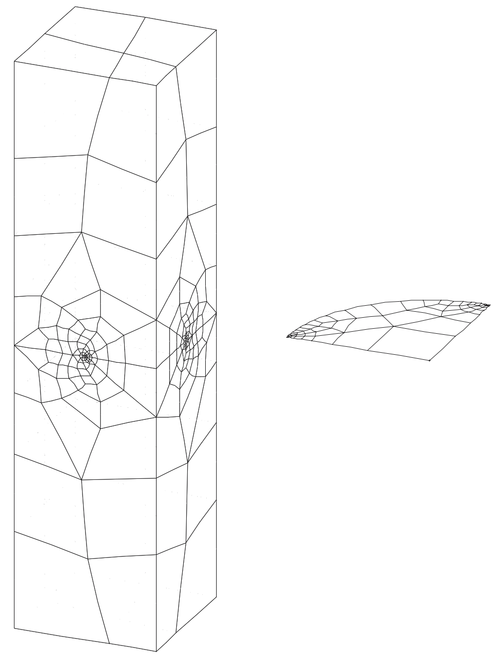

Figure 8 : Mesh of a quarter-circular crack in a square bar for the SGBEM

displacement ones.

This problem is a pure mode-I problem and has been solved by using the FEM [Raju and Newman (1979)] and the SGBEM [Frangi, Novati, Sprinthetti and Rovizzi (2002)]. The analytical solution is available for the infinite plate. The ratios chosen for this prolem are large enough to represent a crack in the infinite plate. As shown in Fig. 6, a comparison of the normalized stress intensity factors by using the SGBEM-FEM alternating method with the referenced solutions shows a good agreement for all crack-front locations. It is well known that that the stress intensity factors tend to zero in a boundary layer where the crack front approaches free surface of the body, when a surface crack breaks the outer surface at a right angle. This effect is also confirmed by using alternating method.

5.2 A quarter-circular crack in a square bar

The second example for the surface crack is a square bar which contains a quarter-circular crack, as shown in Fig. 7. Uniform tensile stresses σ_0 are applied at the two ends. Let a denote the radius of the quarter-circular crack, and the other dimensions are defined as $\frac{w}{a} = 5$ and $\frac{h}{a} = 4$. The Poisson ratio $\nu = 0.3$ is chosen here. The dimensions are chosen to be the same as those used in Li, Mear and Xiao (1998) for comparison purpose.

Again, we use both the SGBEM for the entire domain; and the FEM-SGBEM alternating method to solve this problem with the meshes in Figs. 8 and 9, respectively. The local SGBEM domain is created by truncating the square bar as shown in Fig. 9(a). Then the top and bottom surfaces are subjected to the zero prescribed displacements and others are free.

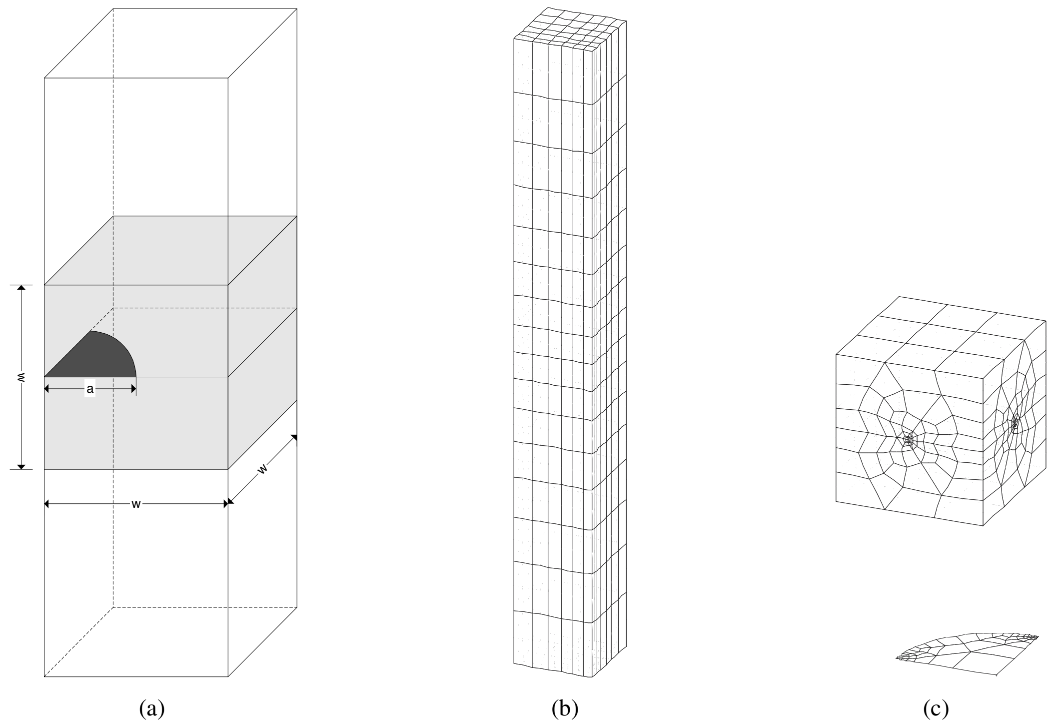

Figure 9 : Models of a quarter-circular crack in a square bar for FEM-SGBEM alternating method: (a) local finite body defined in the plate, (b) the FEM model without the crack and (c) the local SGBEM model with the crack

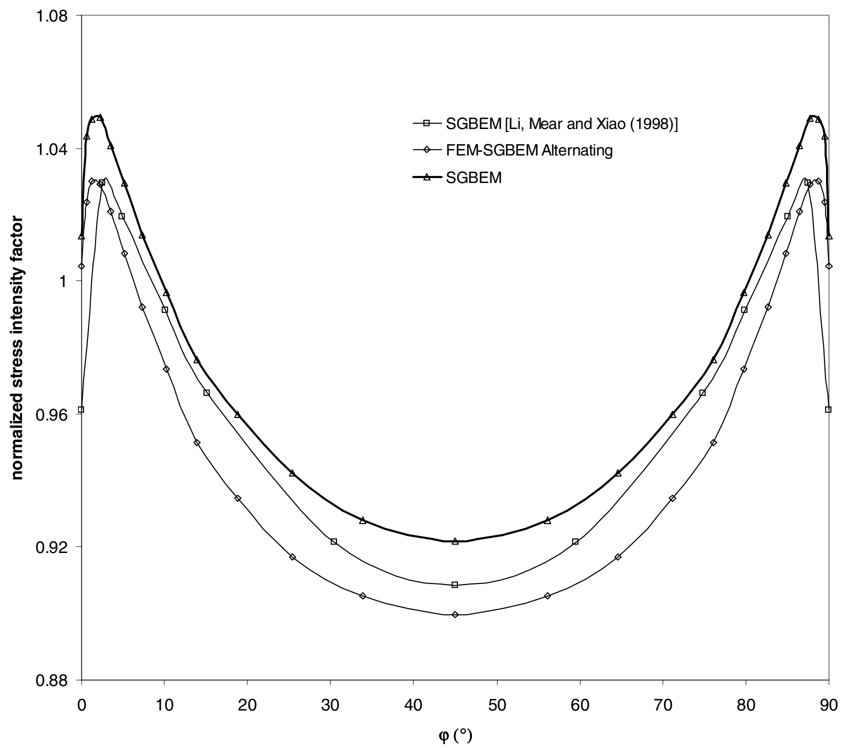

Figure 10 : Normalized stress intensity factors $(K_I/\sigma_0\sqrt{\pi a}))$ for a quarter-circular crack in a square bar

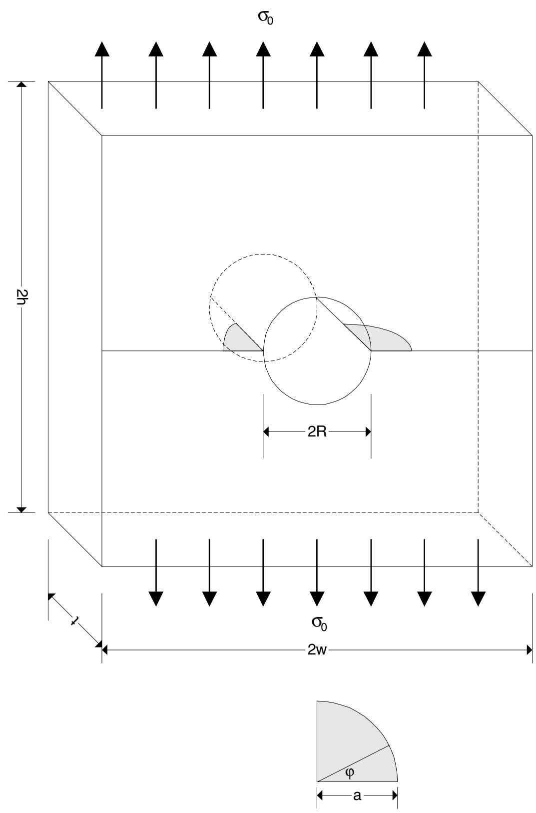

Figure 11 : a corner crack at a circular hole in a finite-thickness plate under tension

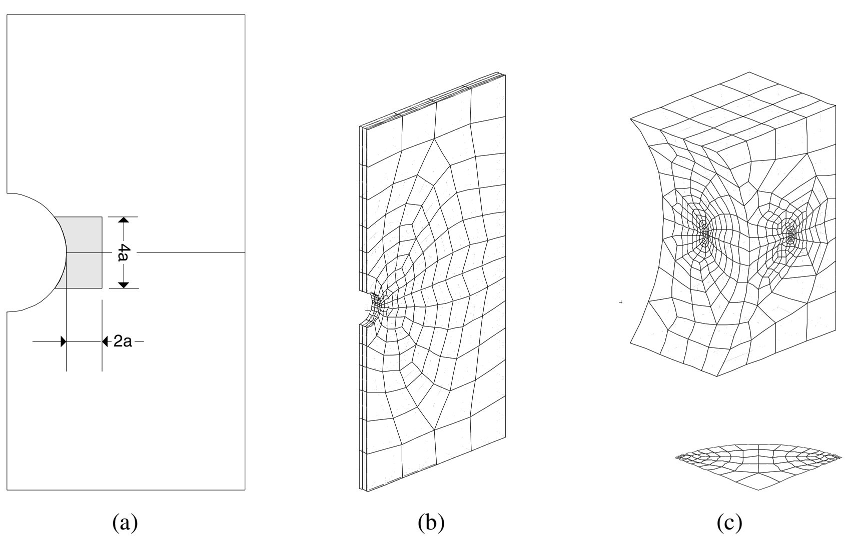

Figure 12 : Models of a corner crack at a circular hole in a finite-thickness plate for FEM-SGBEM alternating method: (a) local finite body defined in the plate, (b) the FEM model without the crack and (c) the local SGBEM model with the crack

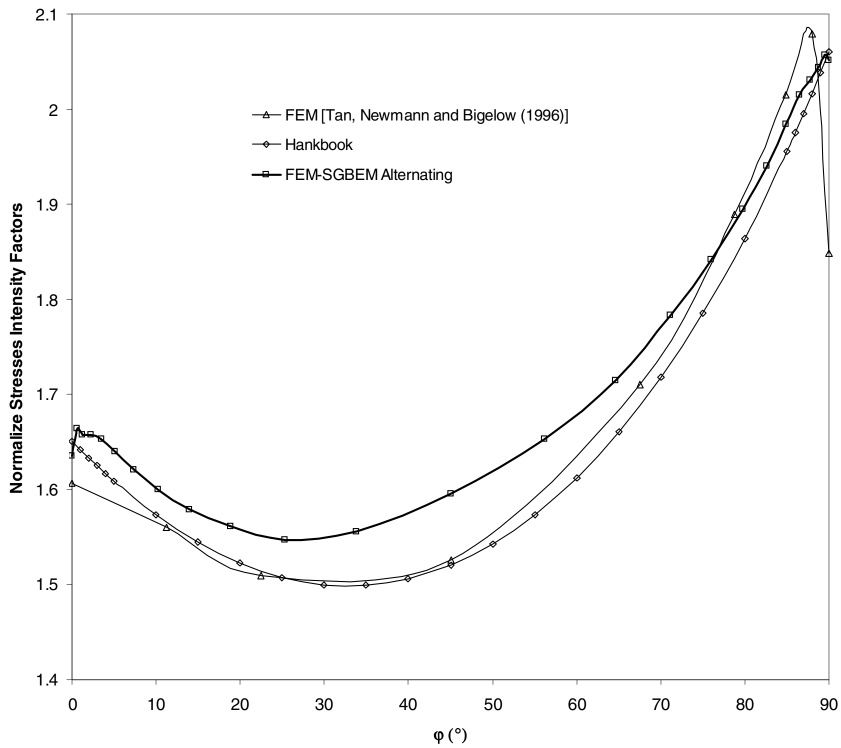

Figure 13 : Normalized stress intensity factors (KI / ($\sigma_0\sqrt{\pi a}$)) for a corner circular crack at a hole in a finite-thickness plate

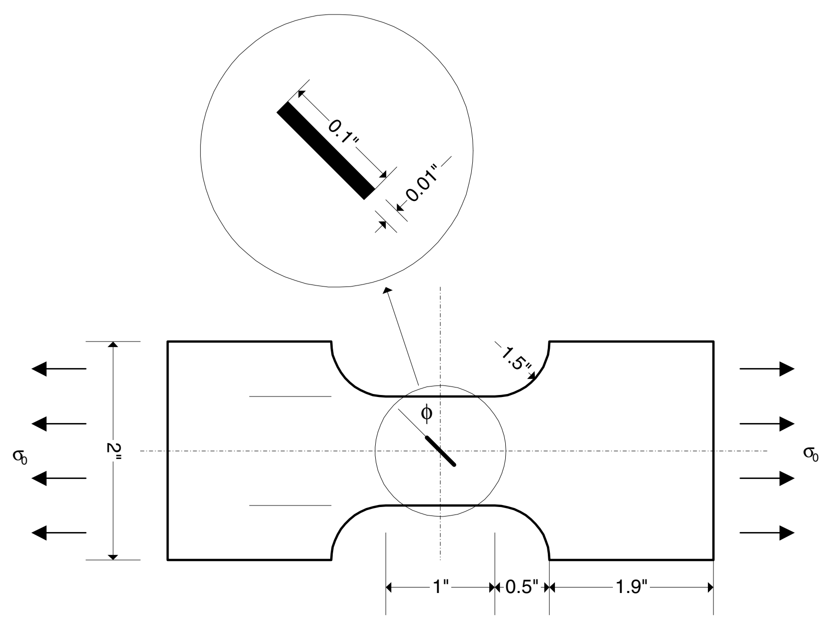

Figure 14 : Inclined semi-circular surface crack specimen

Numerical results are displayed in Fig. 10 in terms of the normalized stress intensity factor contribution along the crack front. A good agreement is observed, as well as those points near the free surface. Again the boundary effect is also evidenced by the alternating method.

5.3 Corner crack at a circular hole in a finite-thickness plate

As the third example, the corner crack at a circular hole in a plate is considered and shown in Fig. 11. This example has been considered by many investigators for three dimensional fracture analyses with various methods. The geometry is characterized by the ratios: $\frac{h}{t} = \frac{w}{t} = 8$, $\frac{R}{t} = 1.5$ and $\frac{a}{t} = 0.5$. The passion ratio is taken as $\nu = 0.3$.

This problem is analyzed by using the alternating method only. The meshes adopted are depicted in Fig. 12(b)-(c), in which only half of the specimen was analyzed due to symmetry. The FEM model has about 3300 degrees of freedom (DOFs). In the contrast, the FEM models used in Tan, Newman and Bigelow (1996) had more than 16000 DOFs in conjunction with special singularity elements for the crack front. The local SGBEM model is cut by three planar surfaces around the crack with zero prescribed displacements, as shown in Fig. 12 (a). All boundary and crack surfaces are discretized with about 500 quadrilateral elements, and with 24 elements along the crack front.

The normalized stress intensity factors along the crack front are plotted in Fig. 13. The results are compared to the available published solutions [Tan, Newman and Bigelow (1996)]. The boundary effects are obtained for two ends of the crack front near to the free surface, and the boundary layer at the lateral free surface is thinner than the FEM solution.

5.4 Nonplanar fatigue growth of an inclined semi-circular surface crack in a plate

Fatigue-growth of an inclined surface crack in a plate is considered. As shown in Fig. 14, the modified ASTM E740 specimen has been tested for the mixed-mode fatigue growth [Forth, Keat and Favrow (2002)]. The specimens were taken from actual parts made from 7075-T73 aluminum. The crack orientation $\phi = 30°$ is used. Maximum tensile stresses $\sigma_0 = 15.88 ksi$ are applied with a load ratio $R = 0.7$. The Forman equation is chosen to advance the crack and front and determine the fatigue cycles:

$$\frac{da}{dN} = C\left(\frac{1-f}{1-R}\Delta K\right)^n \frac{(1-\Delta K_{th}/\Delta K)^p}{(1-K_{\max}/K_{crit})^q} \tag{32}$$

where the growth rate $\frac{da}{dN}$ is based on empirical material constants$C$, n, p and q; f depends on the ratio R; ΔK_{th} is the threshold value of ΔK; K_{crit} is the critical stress intensity factor. This model is details in the reference manual of NASGARO 3.0 [NASA, NASGRO (2001)]. The material constants are taken as $C = 1.49 \times 10^{-8}$, $n = 3.321$, $p = 0.5$, $q = 1.0$, $K_{Ie} = 50 ksi\sqrt{in}$, $K_{IC} = 28 ksi\sqrt{in}$, $\Delta K_{th} = 3.0 ksi\sqrt{in}$, $C_{th}^{+} = 2.0$, $C_{th}^{-} = 1.0$, $R_{cl} = 0.7$,$\alpha = 1.9$, $A_k = 1.0$, $B_k = 1.0$, $S_{\max}/\sigma_0 = 0.3$, $\sigma_{YS} = 60 ksi$ and $\sigma_{UTS} = 74 ksi$.

We model the uncracked specimen with the mesh as in Fig. 15b for FEM. The local SGBEM model is located in the central portion that contains the inclined surface crack, as illustrated in Fig. 15a with the attendant mesh being shown in Fig. 15c. The top and bottom surfaces are cutting surfaces and subjected to the zero prescribed displacements while others are free.

First, the initial crack is analyzed and stress intensity factors are normalized by $K_0 = \sigma_0\sqrt{\pi a}$ and shown in Fig. 16. Good agreements are obtained in comparison with other results [Shivakumar and Raju (1992); He and Hutchinsen (2000); Nikishkov, Park and Atluri (2001)].

The crack growth is simulated by adding one layer of elements along the crack front, in each increment. The newly added points are determined through the K solutions. 15 advancements are performed. The fatigue load cycles are calculated and compared with the experimental data [Forth, Keat and Favrow (2002)], shown in Fig. 17. The normalized stress intensity factors during the crack growing are given in Fig. 18, which are also normalized by $K_0 = \sigma_0\sqrt{\pi a}$. KI keeps increasing while KII and KIII are decreasing during the crack growth. It confirms that this mixed-mode crack becomes the mode-I dominated one while growing. The shape of the final crack is very similar to the experimental photograph in Fig. 19. It is clear that while the crack, in its initial configuration, starts out as a mixed-mode crack, after a substantial growth, the crack configuration is such that it is in a pure mode-I state.

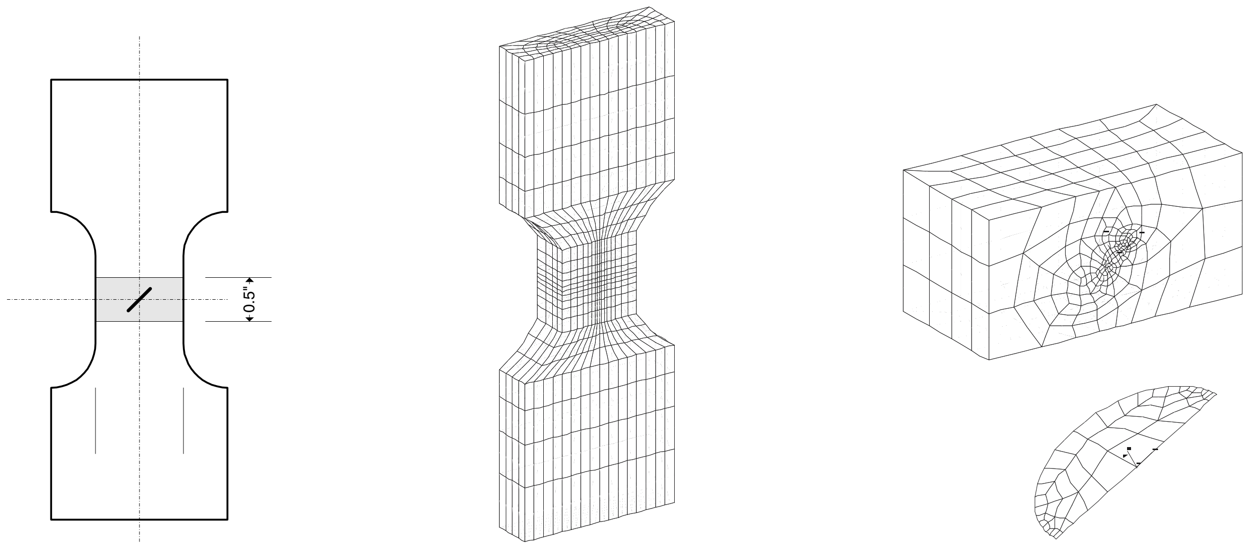

(a) (b) (c)

Figure 15 : Models of an inclined surface crack in a tensile plate for FEM-SGBEM alternating method: (a) local finite body defined in the specimen, (b) the FEM model for the specimen without the crack and (c) the local SGBEM model with the crack

5.5 Automatic detection of an initial nozzle corner flaw

As the final example, the initial crack at a nozzle corner is detected by using the program DTALE, which employs the present alternating method. The geometries of the nozzle and of the flaw in a longitudinal plane are shown in Fig. 20. Two types of initial flaws, as shown in Fig. 21, one a quarter-circular flaw (MATH) of depth a =9.5cm and a similar “natural” flaw (EXPR) obtained in a photoelastic test [Smith, Jolles and Peters (1976)] were assumed in the damage tolerance analysis. In most analyses, the experimental results are not available. The shape, size and orientation of the initial flaw need to be assumed based on the users’ experience, which is not easy. An alternative way is to do the parametric study by creating many initial flaws based on the combination of the parameters of the shape, size, and orientation. From the computational point of view, it is not efficient, if other parameters are also considered including load cases and boundary conditions.

In the present study, one may determine the initial flaw by utilizing the automatic crack-growth function in DTALE. At the beginning, a smaller initial crack is introduced as the crack seed, and the program grows the crack seed with the same loading and boundary conditions. The present study, the Walker’s fatigue model is used to grow the crack seed, without the threshold value of the stress intensity factor. After several advancements of the crack seed, the larger crack flaw can be obtained with the proper shape and orientation. As shown in Fig. 21, an initial crack seed is given as the black portion. The automatically detected portion of the initial flaw is shown in gray, which agrees with the experimental results. The fatigue model for the small crack can be used here for more accurate initial crack detection, because it fits the development of the initial crack well.

6 Conclusions

In this paper the Schwartz-Neumaan alternating method has been extended to analyze surface cracks. It is shown that the singular traction integral is avoided during the alternating procedure between the FEM and SGBEM, when both solutions are based on finite bodies. This approach shows a strong computational competitiveness, in comparison to the normal alternating methods, by avoiding the stress calculation on the boundary surfaces of FEM models. Indeed, the alternating procedure converges unconditionally by imposing the proposed prescribed displacements and tractions in the present approach. The accuracy and efficiency of the proposed approach have been verified on some 3D problems with published solutions by using other methods. The soft-

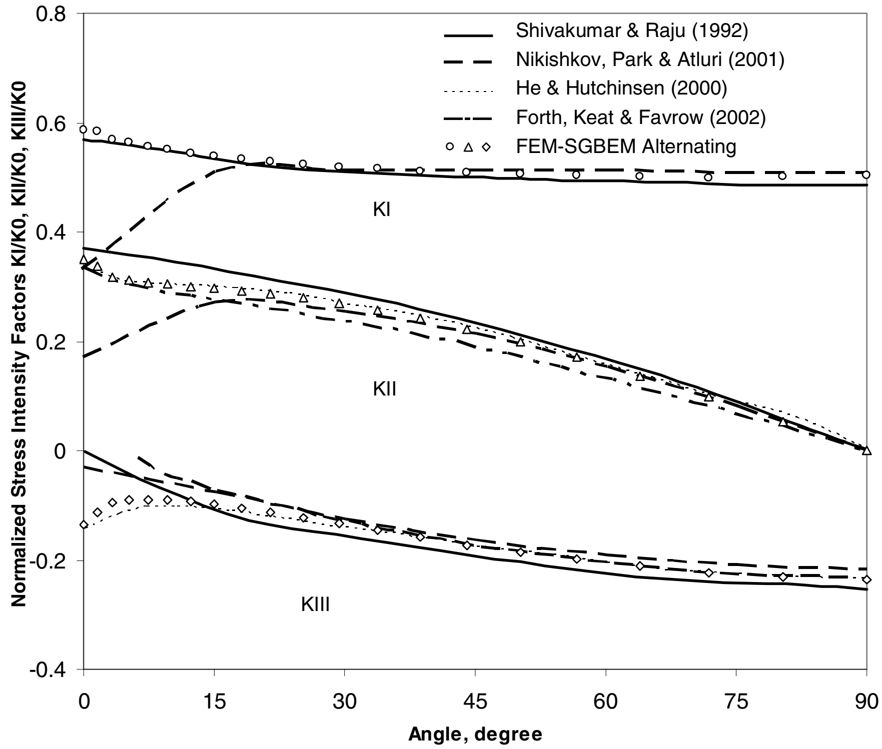

Figure 16 : Normalized stress intensity factors KI, KII and KIII for an inclined semi-circular surface crack in a tensile plate

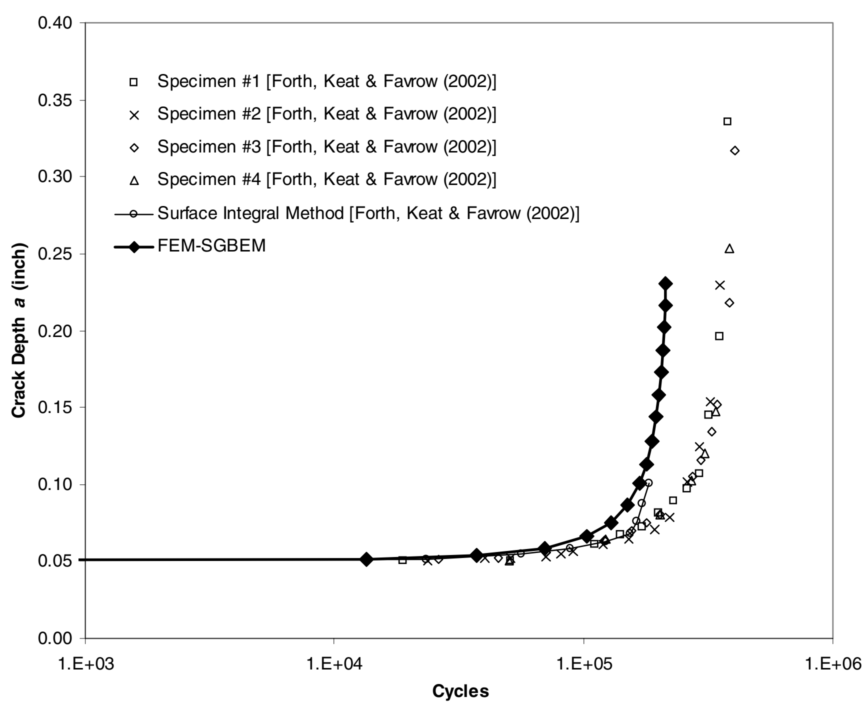

Figure 17 : Fatigue load cycles of an inclined semi-circular surface crack in a tensile plate

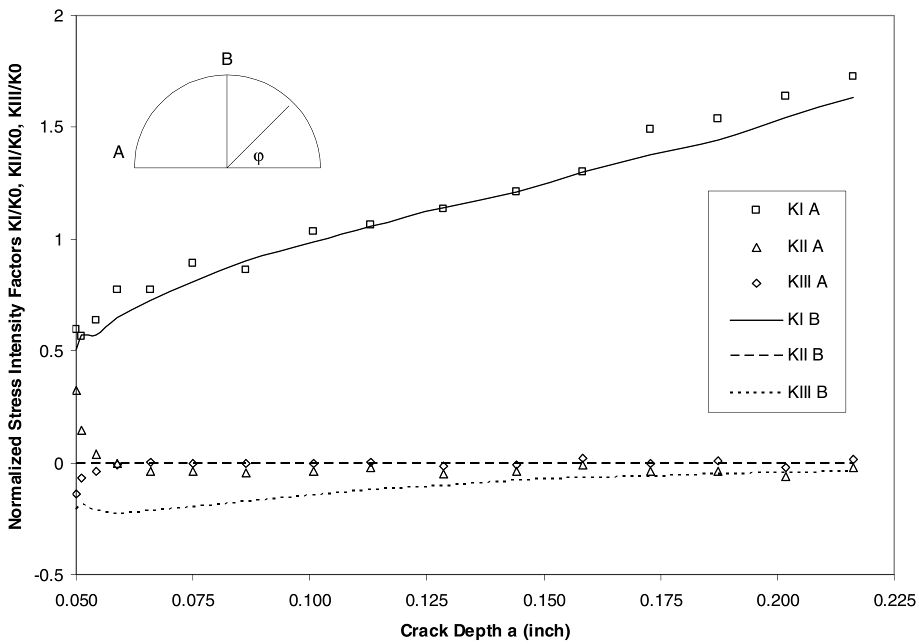

Figure 18 : Normalized stress intensity factors KI, KII and KIII for the mixed-mode fatigue growth of an inclined semi-circular surface crack in a tensile plate

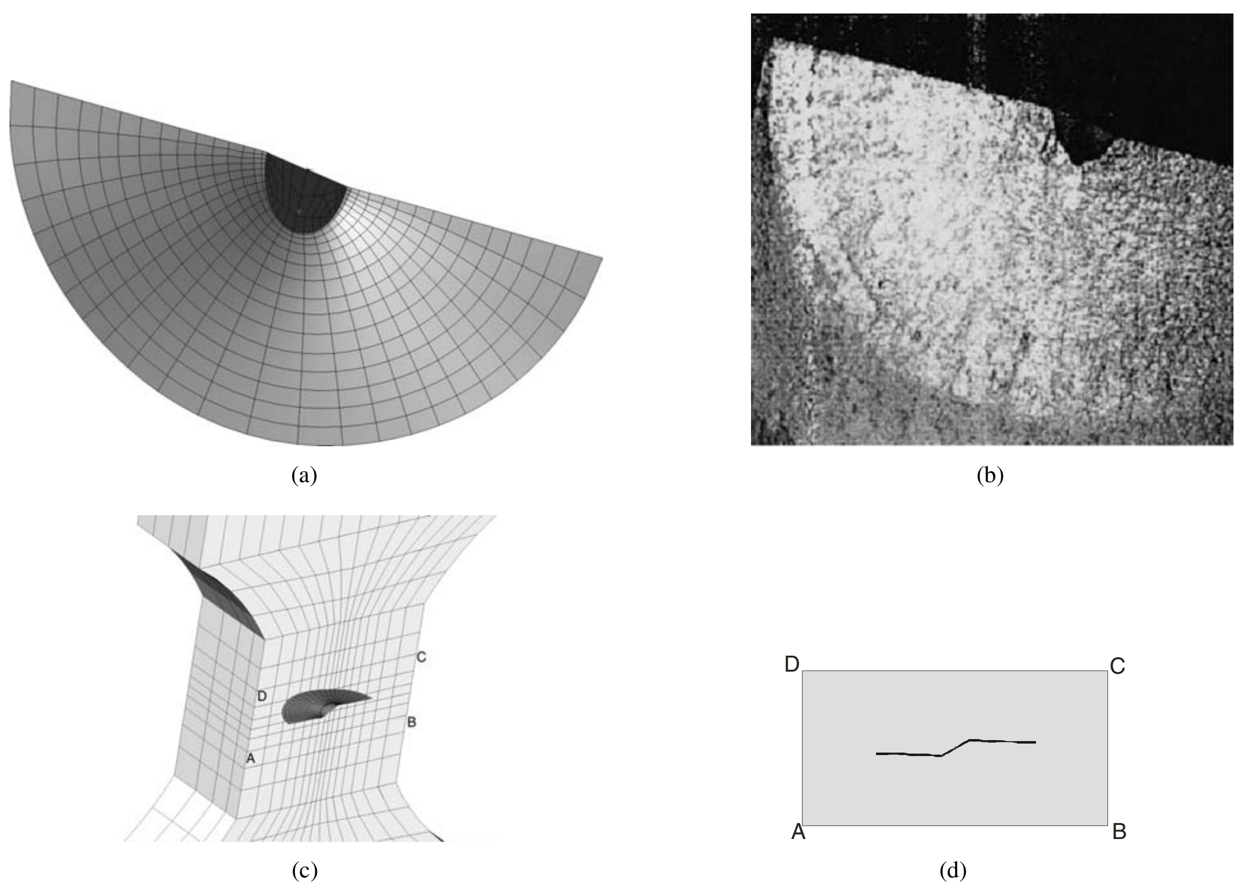

Figure 19 : Final crack of an inclined surface crack in a tensile plate: (a) the final crack after 15 increments by using FEM-SGBEM alternating method, (b) the photograph of the final crack taken from the specimen, (c) the final crack in the uncracked body, (d) the intersection path of the final crack with the free surface of the specimen, ABCD

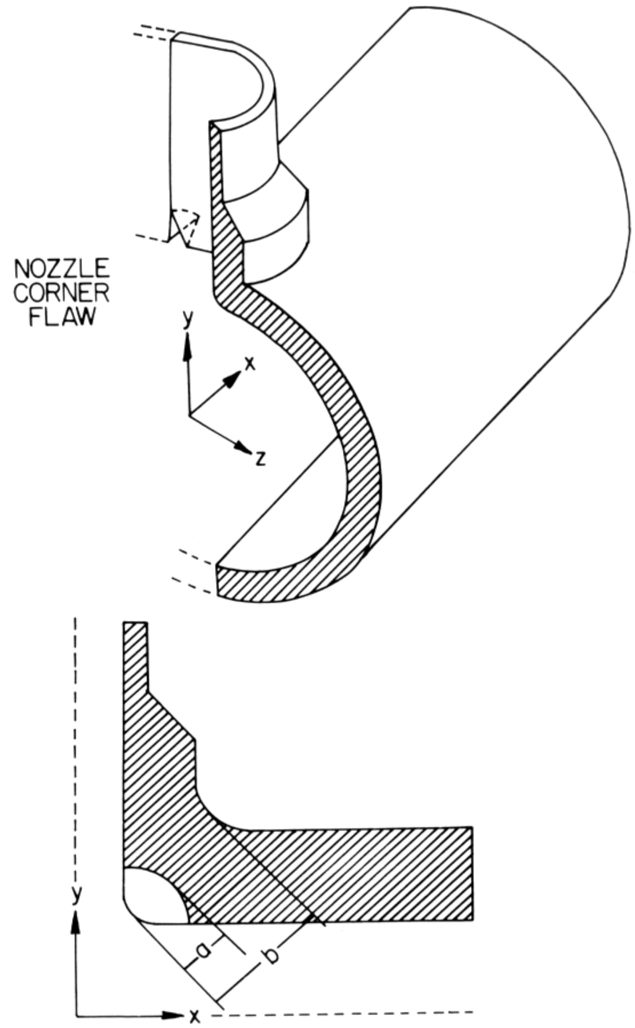

Figure 20 : Surface-flaw near a pressure-vessel-nozzle junction

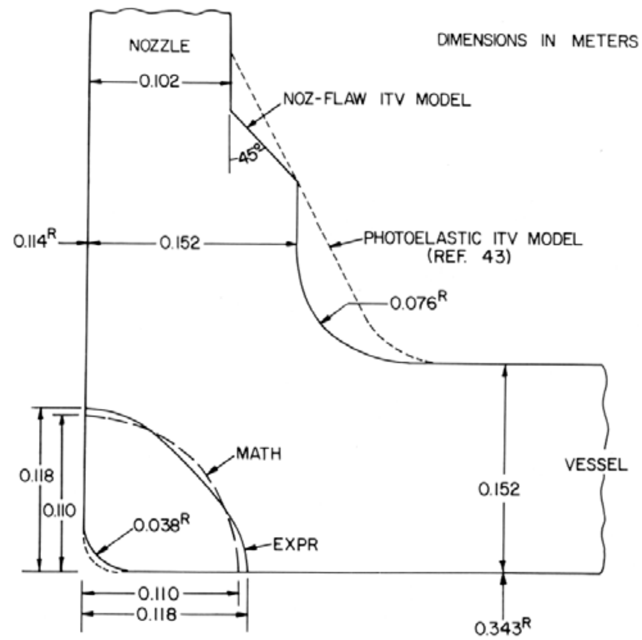

Figure 21 : Geometry of an intermediate-test-vessel nozzle configuration

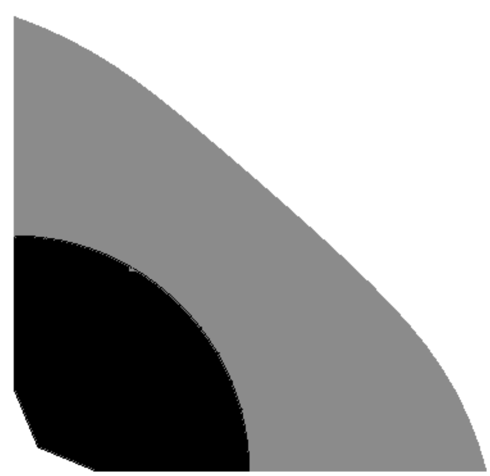

Figure 22 : Automatic initial crack detection

ware pacakge, DTALE, has been developed based on the present method. DTALE can be seen to have a wide industrial application, in estimating the life of a variety of safety-critical structures. With DTALE, the effect of residual stresses in a structure, due to processes such as welding, cold-working, shot-peening, etc., on the life of the structure, including a possible life-enhancement, can also be assessed.

References

Andra, H. (1998): Integration of singular integrals for the Galerkin-type boundary element method in 3D elasticity. Comp. Methods Appl. Mech. Engng, vol. 157, pp. 239-249.

Atluri, S.N (2004): *The Meshless Local Petrov-Galerkin (MLPG) Method for Domain & Boundary Discretizations*, Tech Science Press, 680 pages.

Atluri, S. N. (1997): Structural Integrity and Durability, Tech Science Press, Forsyth.

Atluri, S. N. (1986): Computational Methods in the mechanics of fracture (North Holland, Amsterdam) also translated into Russian, Mir Publishers, Moscow.

Atluri, S. N.; Han, Z. D.; Shen, S.(2003): Meshless Local Patrov-Galerkin (MLPG) approaches for weakly-singular traction & displacement boundary integral equations, CMES: *Computer Modeling in Engineering & Sciences*, vol. 4, no. 5, pp. 507-517.

Atluri, S. N.; Kathireasan, K. (1975): An assumed displacement hybrid finite element model for three-dimensional linear elastic fracture mechanics analysis. Presented at the 12^{th} Annual Meeting of the Society of Engineering Science, University of Texas, Austin.

Cisilino, A.P.; Aliabadi, M.H. (1999): Threedimensional boundary element analysis of fatigue crack growth in linear and non-linear fracture problems. Eng. Fract. Mech., vol. 63, pp. 713-733.

Forth, S. C.; Keat W. D.; Favrow L. H. (2002): Experimental and computational investigation of three-dimensional mixed-mode fatigue, Fatigue Fract. Engng. Mater. Struct., vol. 25, pp 3-15.

Erichsen, S.; Sauter, S.A. (1998): Efficient automatic quadrature in 3-d Galerkin BEM. Com. Methods Appl. Mech. Engng, vol. 157, pp. 215-224.

Frangi, A.; Novati, G. (2002): Fracture mechanics in 3D by a coupled FE-BE approach, IABEM 2002, International Association for Boundary Element Methods, UT Austin, Texas, May 28-30.

Frangi, A; Novati, G.; Sprinthetti, R.; Rovizzi, M. (2002): 3D fracture analysis by the symmetric Galerkin BEM, Computational Mechanics, vol. 28, pp. 220-232.

Han. Z. D.; Atluri, S. N. (2002): SGBEM (for Cracked Local Subdomain) - FEM (for uncracked global Structure) Alternating Method for Analyzing 3D Surface Cracks and Their Fatigue-Growth, CMES: *Computer Modeling in Engineering & Sciences*, vol. 3 no. 6, pp. 699-716.

Han. Z. D.; Atluri, S. N. (2003a): On Simple Formulations of Weakly-Singular Traction & Displacement BIE, and Their Solutions through Petrov-Galerkin Approaches, CMES: *Computer Modeling in Engineering & Sciences*, vol. 4 no. 1, pp. 5-20.

Han. Z. D.; Atluri, S. N. (2003b): Truly Meshless Local Petrov-Galerkin (MLPG) Solutions of Traction & Displacement BIEs, CMES: *Computer Modeling in Engineering & Sciences*, vol. 4 no. 6, pp. 665-678.

Han. Z. D.; Atluri, S. N. (2004a): Meshless Local Petrov-Galerkin (MLPG) approaches for solving 3D Problems in elasto-statics, CMES: *Computer Modeling in Engineering & Sciences*, vol. 6 no. 2, pp. 169-188.

Han. Z. D.; Atluri, S. N. (2004b): A Meshless Local Petrov-Galerkin (MLPG) Approach for 3-Dimensional Elasto-dynamics, CMC: *Computers, Materials & Continua*, vol. 1 no. 2, pp. 129-140.

He, M. Y.; Hutchinson, J. W. (2000): Surface crack subject to mixed mode loading. Engng. Fract. Mech. 65, 1–14.

Kantorovich, L. V.; Krylov, V. I. (1964): Approximate methods of higher analysis (translated by Curtis D. Benster) (John Wiley & Sons, Inc., New York &London).

Keat, W.D.; Annigeri, B.S.; Cleary, M.P. (1988): Surface integral and finite element hybrid method for twoand three-dimensional fracture mechanics analysis. Int. J. Fracture, vol. 36, pp. 35-53.

Murakami, Y. (1987): Stress Intensity Factors Handbook, Pergamon Press.

NASA (2001), The reference manual of fatigue crack growth computer program "NASGRO" version 3.0, JSC-22267B, Nov. 2001.

Nikishkov, G.P.; Atluri, S.N. (1987): Calculation of fracture mechanics parameters for an arbitrary threedimensional crack by the "equivalent domain integral" method. Int. J. Numer Meth. Engng, vol. 24, pp. 851-867.

Nikishkov, G.P.; Park, J.H.; Atluri, S. N. (2001): SGBEM-FEM alternating method for analyzing 3D non-planar cracks and their growth in structural components, CMES: Computer Modeling in Engineering & Sciences, vol.2, no.3, pp.401-422.

Nishioka, T.; Atluri, S.N. (1983): Analytical solution for embedded elliptical cracks and finite element alternating method for elliptical surface cracks, subjected to arbitrary loadings. Eng. Fract. Mech., vol. 17, pp. 247-268.

Okada, H.; Atluri, S. N. (1994): Recent developments in the field-boundary element method for finite/small strain elastoplasticity, *Int. J. Solids Struct*. vol. 31 n. 12-13, pp. 1737-1775.

Okada, H.; Rajiyah, H.; Atluri, S. N. (1989)a: A Novel Displacement Gradient Boundary Element Method for Elastic Stress Analysis with High Accuracy, *J. Applied Mech*., April 1989, pp. 1-9.

Okada, H.; Rajiyah, H.; Atluri, S. N. (1989)b: Non-hyper-singular integral representations for velocity (displacement) gradients in elastic/plastic solids (small or finite deformations), *Comp. Mech.*, vol. 4, pp. 165-175.

Okada, H.; Rajiyah, H.; Atluri, S. N. (1990): A full tangent stiffness field-boundary-element formulation for geometric and material non-linear problems of solid mechanics, *Int. J. Numer. Meth. Eng.*, vol. 29, no. 1, pp. 15-35.

Raju, I. S.; Newman, J. C. Jr (1979): Stress-intensity factors for a wide range of semi-elliptical surface cracks in finite-thickness plates, Engineering Fracture Mechanics, vol. 11, pp. 817-829.

Shivakumar, K.N.; Raju, I.S. (1992): An equivalent domain integral method for three-dimensional mixed-mode fracture problems. Eng. Fract. Mech., vol. 42, pp. 935-959.

Smith, C. W.; Jolles, M.; and Peters, W. H. (1976): Stress intensities of nozzle cracks in reator vessels, VPI-E-76-25, ORNL/SUB-7015/1 (Virginia Polytechnic and State Univ.)

Tan, P. W.; Newman, J. C. Jr.; Bigelow, C. A. (1996): Three-dimensional finite-element analyses of corner cracks at stress concentrations, Engineering Fracture Mechanics, vol. 55, no. 3, pp. 505-512.

Vijaykumar, K.; Atluri, S.N. (1981): An embedded elliptical crack, in an infinite solid, subject to arbitrary crack-face tractions, J. Appl. Mech., vol. 103(1), pp. 88-96.

Wang, L.; Atluri, S.N. (1996): Recent Advances in the alternating methods for elastic and inelastic fracture analyses, Computer methods in Applied Mechanics and Engineering, vol. 137, pp. 1-57.